The steady oblique path of buoyancy-driven disks and spheres

David Fabre[1],
Joël Tchoufag[1] **and Jacques Magnaudet**[1,2]

[1]Université de Toulouse; INPT, UPS; IMFT (Institut de Mécanique des Fluides de Toulouse); Allée Camille Soula, F-31400 Toulouse, France.
[2]CNRS; IMFT; F-31400 Toulouse, France.

(Received 6 February 2012)

We consider the steady motion of disks of various thicknesses in a weakly viscous flow, in the case where the angle of incidence α (defined as that between the disk axis and its velocity) is small. We derive the structure of the steady flow past the body and the associated hydrodynamic force and torque through a weakly nonlinear expansion of the flow with respect to α. When buoyancy drives the body motion, we obtain a solution corresponding to an oblique path with a nonzero incidence by requesting the torque to vanish and the hydrodynamic and net buoyancy forces to balance each other. This oblique solution is shown to arise through a bifurcation at a critical Reynolds number Re^{SO} which does not depend upon the body-to-fluid density ratio and is distinct from the critical Reynolds number Re^{SS} corresponding to the steady bifurcation of the flow past the body held fixed with $\alpha = 0$. We then apply the same approach to the related case of a sphere that weakly rotates about an axis perpendicular to its path and show that an oblique path sets in at a critical Reynolds number Re^{SO} slightly lower than Re^{SS}, in agreement with available numerical studies.

Key words: flow-structure interactions, bifurcation.

1. Introduction

The dynamics of bodies freely falling or rising within a viscous fluid under the effect of buoyancy is currently an active field of research (see Ern *et al.* (2012) for a recent review). A large variety of paths has been reported, including fluttering, tumbling, spiral and chaotic motions. In some cases, such as light spheres (Jenny, Dusek & Bouchet 2004) and thin disks with a density close to that of the fluid (Fernandes *et al.* 2007; Auguste 2010), a number of regimes characterized by weak deviations with respect to the vertical (collectively termed A-regimes by Ern *et al.*) have been noticed at Reynolds numbers significantly smaller than those for which large-amplitude oscillatory lateral motions (fluttering) are observed. The first of these non-vertical paths consists of a steady oblique (SO) trajectory, the body being slightly tilted with respect to its path (for a disk) or slowly rotating (for a sphere). In such states, the wake is characterized by the presence of a pair of steady counter-rotating streamwise vortices (Jenny *et al.* 2004; Horowitz & Williamson 2010). This structure suggests that this SO path is strongly connected to the steady-state (SS) mode observed after the first wake bifurcation in the related problem of the flow past a fixed, untilted (or non-rotating) body, e.g. Fabre, Auguste & Magnaudet (2008); Meliga, Chomaz & Sipp (2009); Chrust, Bouchet & Dusek

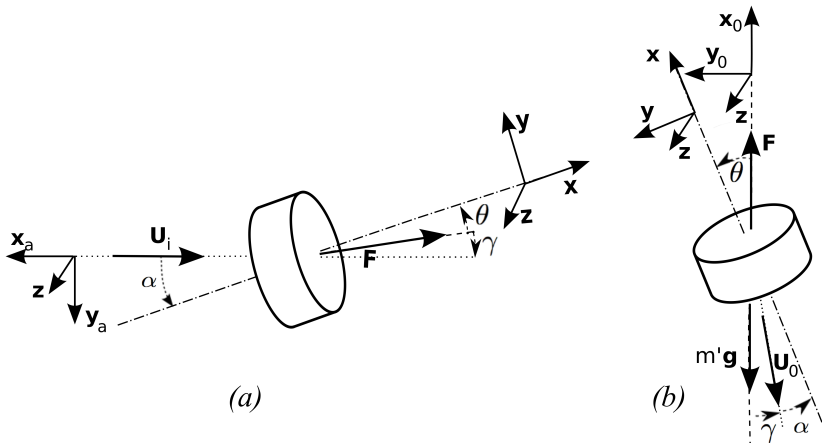

FIGURE 1. Sketch of the problem. (a) fixed body; (b) freely-moving body ($[\mathbf{x}_0, \mathbf{y}_0, \mathbf{z}]$ is the laboratory system of axes and $m'\mathbf{g}$ the net body weight). α (resp. θ) is the angle between the incoming velocity $\mathbf{U_i} = -\mathbf{U_0}$ (resp. the hydrodynamic force $\mathbf{F}$) and the body axis $\mathbf{x}$, while $\gamma = \theta - \alpha$ is the angle between $\mathbf{F}$ and the incoming velocity (γ is negative in (a) and positive in (b)). Note that, owing to the convention defined in (2.2), the lift component L of $\mathbf{F}$ is positive in (a) and negative in (b).

(2010). However, differences have been noticed between the values of the critical Reynolds number associated with the onset of the SO path and that of the SS mode. Also, it is not clear whether or not the former critical Reynolds number depends on the body-to-fluid relative density which is an additional control parameter when the body moves freely.
The goal of this paper is to derive an approximate solution for the flow around the body through a weakly-nonlinear expansion of the Navier-Stokes equations, the force and torque being expanded in Taylor series with respect to the angle of incidence. We first describe the general method in the case of a slightly tilted disk of arbitrary thickness. Then we show that an equilibrium solution for a freely-moving disk with nonzero incidence and nonzero inclination with respect to the vertical can be constructed, and emerges through a supercritical bifurcation (except when the disk is infinitely thin, in which case the bifurcation is found to be subcritical) at a critical Reynolds number independent of the body-to-fluid density ratio. We finally apply the same approach to a sphere, the expansion then being carried out with respect to the rotation rate.

2. A weakly nonlinear expansion for the flow past a fixed body with a small imposed incidence

2.1. *Problem definition*

We consider a cylindrical body of diameter d and thickness h moving steadily at a velocity $\mathbf{U_0}$ in a quiescent viscous fluid, or equivalently the same body held fixed in a uniform flow of incoming velocity $\mathbf{U}_i = -\mathbf{U}_0$. The problem in this section is to compute the steady flow $[\mathbf{u}, p]$ past this body and deduce the corresponding force and torque $(\mathbf{F}, \mathbf{M})$. We define two systems of axes similar to those employed by Fabre, Assemat & Magnaudet (2011) (see figure 1). The first of these, $(\mathbf{x}, \mathbf{y}, \mathbf{z})$, is associated with the body geometry, with $\mathbf{x}$ coinciding with the body axis. The second is the aerodynamic system $(\mathbf{x}_a, \mathbf{y}_a, \mathbf{z})$, where $\mathbf{x}_a$ is aligned with the body velocity $\mathbf{U_0}$. Introducing the angle of incidence α between $\mathbf{U_i}$ and the body axis $\mathbf{x}$, one has

$$\mathbf{U}_i = -U_0 \mathbf{x_a} = U_0(\cos\alpha \mathbf{x} - \sin\alpha \mathbf{y}) \quad . \tag{2.1}$$

The hydrodynamic loads can also be projected onto the two systems of axes, yielding axial and lateral force components in the former and drag and lift components in the latter, with

$$\mathbf{F} = -(D\mathbf{x}_a + L\mathbf{y}_a) = F_x\mathbf{x} + F_y\mathbf{y} \quad , \quad \mathbf{M} = M\mathbf{z} \quad , \tag{2.2}$$

the two series of force components being related through

$$D = F_x\cos\alpha - F_y\sin\alpha \quad , \quad L = F_x\sin\alpha + F_y\cos\alpha \quad . \tag{2.3}$$

The velocity field $\mathbf{u}$ and pressure field p satisfy the steady incompressible Navier-Stokes equations which are conveniently written in the form

$$\frac{1}{2}\mathcal{C}(\mathbf{u},\mathbf{u}) + \frac{1}{\rho}\nabla p - \nu\nabla^2\mathbf{u} = 0 \quad , \quad \nabla\cdot\mathbf{u} = 0 \quad , \tag{2.4}$$

where $\mathcal{C}(\mathbf{a},\mathbf{b}) = \mathbf{a}\cdot\nabla\mathbf{b} + \mathbf{b}\cdot\nabla\mathbf{a}$ is the symmetric advection operator, ρ and ν being the fluid density and kinematic viscosity, respectively. The boundary equations to be satisfied by $\mathbf{u}$ are the no-slip condition $\mathbf{u} = \mathbf{0}$ at the body surface and the matching with the incoming flow at infinity, i.e. $\mathbf{u} \to \mathbf{U}_i$ as $|\mathbf{R}| \to \infty$, $\mathbf{R}$ denoting the local position from the body centre of mass. Once the flow field is known, the hydrodynamic force and torque are evaluated as

$$\mathbf{F} = \int_S (-p\mathbf{n} + \rho\nu(\nabla\mathbf{u} + \nabla\mathbf{u}^T)\cdot\mathbf{n})dS \ , \quad \mathbf{M} = \int_S \mathbf{R}\times(-p\mathbf{n} + \rho\nu(\nabla\mathbf{u} + \nabla\mathbf{u}^T)\cdot\mathbf{n})dS \ , \tag{2.5}$$

where $\mathbf{n}$ is the outward unit normal to the body surface. These loads may be represented through the classical aerodynamic coefficients defined as

$$[L, D, F_x, F_y] = \frac{\rho S U_0^2}{2}[C_L, C_D, C_x, C_y] \quad ; \quad M = \frac{\rho S d U_0^2}{4} C_M \quad , \tag{2.6}$$

where $S = \pi d^2/4$ is the body cross-sectional area. The whole problem may be characterized by the Reynolds number $Re = U_0 d/\nu$ and the body aspect ratio $\chi = d/h$. In the rest of this section we set $U_0 = 1$, $d = 1$, $\rho = 1$, so that $Re = \nu^{-1}$.

2.2. *Weakly nonlinear expansion*

We now expand the state vector $\mathbf{q} \equiv [\mathbf{u}, p]^T$ in the form

$$\mathbf{q} = \mathbf{q}_0 + \alpha\mathbf{q}_\alpha + \alpha^2\mathbf{q}_{\alpha^2} + \alpha^3\mathbf{q}_{\alpha^3} + ... \tag{2.7}$$

Injecting this ansatz into the Navier-Stokes equations results in a set of equations that must be solved at each order, along with appropriate boundary conditions. For this purpose the boundary condition at infinity is also expanded in powers of α, yielding

$$\mathbf{u} \to \mathbf{U}_i = \mathbf{x} - \alpha\mathbf{y} - \frac{1}{2}\alpha^2\mathbf{x} + \frac{1}{6}\alpha^3\mathbf{y} + ... \quad \text{for} \quad |\mathbf{R}| \to \infty \quad . \tag{2.8}$$

Symmetry considerations indicate that even terms in (2.7) can only result in an axial force, while odd terms only contribute to the lateral force and to the torque. Therefore the loads can be anticipated to have the form

$$F_x \approx F_{x0} + \alpha^2 F_{x,\alpha^2} + ... \ , \quad F_y \approx \alpha F_{y,\alpha} + \alpha^3 F_{y,\alpha^3} + ... \ , \quad M \approx \alpha M_\alpha + \alpha^3 M_{\alpha^3} + ... \tag{2.9}$$

The numerical approach used to compute the successive terms in (2.7) is adapted from that of Meliga *et al.* (2009). We first introduce the polar system of axes $(\mathbf{e}_r, \mathbf{e}_\varphi)$ in the (y,z)-plane, so as to write the velocity field in the form $\mathbf{u} = [u_r, u_\varphi, u_x]^T$. Thanks to the modal expansion in the azimuthal direction φ, each problem then becomes two-dimensional in the (r,x)-plane. The finite element FreeFem++ software is used to discretize the differential operators involved in the successive problems. The resulting linear

systems are solved with the UMFPack solver embedded in FreeFem++. A grid made of triangular elements is generated using a Delaunay-Voronoi algorithm, with local refinement at the corners of the body and in its near wake. The computational domain is a rectangle defined by $(r,x)\in[0,r_\infty]\times[x_{-\infty},x_\infty]$ (as displayed in figure 1 of Meliga *et al.*), where $r_\infty, x_{-\infty}$ and x_∞ are chosen large enough not to have a discernible influence on the results. The boundary conditions at infinity arising from (2.8) are directly enforced in the inlet plane ($x=x_{-\infty}$) and lateral boundary ($r=r_\infty$), while a zero-traction condition is used in the outlet plane ($x=x_\infty$).

The leading order in the expansion corresponds to the axisymmetric flow past a body having its axis aligned with the incoming flow. This flow satisfies the Navier-Stokes equations (2.4) with $\mathbf{u}_0\to\mathbf{x}$ for $|\mathbf{R}|\to\infty$, and is computed through Newton iteration. The corresponding loads are then deduced from (2.5). As expected, they reduce to an axial force (which in this case coincides with the drag), corresponding to the term F_{x0} in the expansion (2.9). The associated drag coefficient, C_{x0}, is displayed in figure 2*a* for a disk with an aspect ratio $\chi=10$. In the range of Reynolds numbers of interest here, this coefficient is a smoothly decreasing function of Re for all types of bodies.

2.3. *Order 1 problem: linear correction due to a nonzero incidence*

The next order in the expansion (2.7) corresponds to the leading-order correction to the base flow when the body axis is slightly tilted with respect to the incoming velocity. This problem is similar to one of those considered by Fabre *et al.* (2011) with two-dimensional bodies, where the lift and torque coefficients (L_α, M_α) were used to build a 'quasi-static' model relevant to freely-moving bodies in the limit of large body-to-fluid density ratios. At order α, the Navier-Stokes equations and the associated far-field condition read

$$\mathcal{C}(\mathbf{u_0},\mathbf{u}_\alpha)+\nabla p_\alpha - Re^{-1}\nabla^2\mathbf{u}_\alpha=\mathbf{0}\quad,\quad \nabla\cdot\mathbf{u}_\alpha=0\quad,\quad \mathbf{u}_\alpha\to-\mathbf{y}\ \text{ for }|\mathbf{R}|\to\infty\quad. \tag{2.10}$$

We expand the state vector $\mathbf{q}_\alpha$ in the form

$$\mathbf{q}_\alpha=\hat{\mathbf{q}}_1^1 e^{i\varphi}+\overline{\hat{\mathbf{q}}_1^1}e^{-i\varphi}\quad, \tag{2.11}$$

where $\hat{\mathbf{q}}_n^m$ is the complex mode of order α^n associated with an $e^{im\varphi}$ azimuthal variation and the overbar denotes the complex conjugate. The mode $\hat{\mathbf{q}}_1^1$ is then the solution of the linear system

$$\mathcal{A}_1\hat{\mathbf{q}}_1^1=0\quad,\quad \hat{\mathbf{q}}_1^1\to[-1/2,-i/2,0,0]^T\ \text{ for }|\mathbf{R}|\to\infty\quad. \tag{2.12}$$

Here $\mathcal{A}_m$ is the linearized Navier-Stokes operator acting on perturbations with an azimuthal modal expansion of the form $e^{im\varphi}$, i.e.

$$\mathcal{A}_m=\begin{pmatrix}\mathcal{C}_{m,0}(\cdot,\mathbf{u}_0)-Re^{-1}\nabla_m^2 & \nabla_m\\ \nabla_m^T & 0\end{pmatrix}. \tag{2.13}$$

In (2.13), ∇_m is the gradient operator relative to the azimuthal wavenumber m and $\mathcal{C}_{m,n}(\cdot,\mathbf{b})=\mathbf{b}\cdot\nabla(\cdot)+(\cdot)\cdot\nabla\mathbf{b}$ is the advection operator by which the velocity $\mathbf{b}$ of a mode having an azimuthal wavenumber n acts on the velocity of the current mode of azimuthal wavenumber m, as defined in equation (C2) of Meliga *et al.* (2009). The solution of this linear system provides $\mathbf{q}_\alpha$ which in turn yields $F_{y,\alpha}$ and M_α through (2.5). At this order, the lift component is also linear with respect to α, i.e. $L\approx\alpha L_\alpha$, and (2.3) indicates that $L_\alpha=F_{x0}+F_{y,\alpha}$

The solution of the above problem is well-defined as long as the operator $\mathcal{A}_m$ is not singular. As one could have anticipated, the problem corresponding to $m=1$ happens to be singular for $Re=Re^{SS}$, i.e. right at the bifurcation towards the steady-state (SS) wake mode. The first column of table 1 provides the numerical value of Re^{SS} for

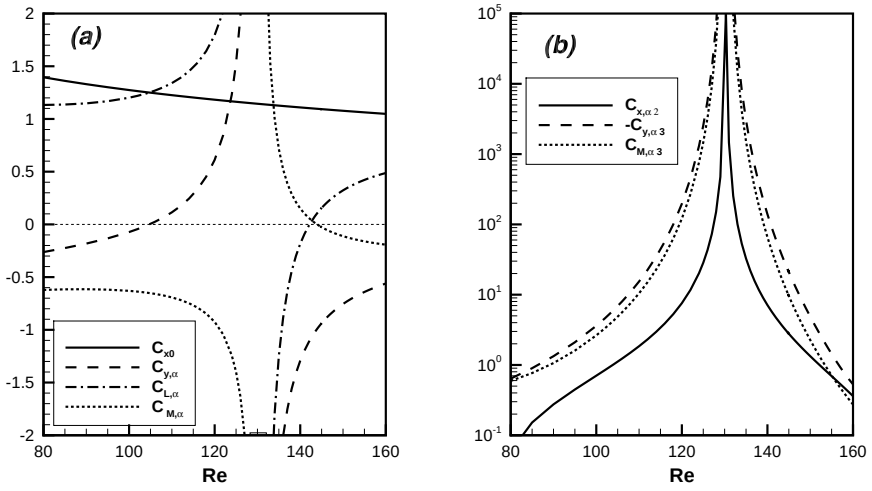

FIGURE 2. Variations with Re of the coefficients entering the weakly nonlinear expansion of loads for a disk with $\chi = 10$; (a) orders 0 and α; (b) orders α^2 and α^3.

disks with three different aspect ratios. The value corresponding to an infinitely thin disk ($\chi = \infty$) is in agreement with that found in previous theoretical and computational studies (Natarajan & Acrivos 1993; Fabre *et al.* 2008; Meliga *et al.* 2009); the values for the other two aspect ratios agree with the results of Chrust *et al.* (2010).

Figure 2a displays the variations with the Reynolds number of coefficients $C_{L,\alpha}, C_{y,\alpha}$ and $C_{M,\alpha}$ corresponding to the loads induced by the above mode $m = \pm 1$ for a disk with an aspect ratio $\chi = 10$. Not surprisingly, the loads tend to infinity as the Reynolds number approaches the critical value $Re = Re^{SS}$, and display a singularity of order one there (i.e. they diverge as $(Re - Re^{SS})^{-1}$). For small enough Reynolds numbers ($Re \lesssim 105$) the lateral projection of the force is negative ($C_{y,\alpha} < 0$) while the lift coefficient $C_{L,\alpha}$ is positive. According to figure 1, this means that the direction of the force lies in between that of the body axis and the incoming flow ($\theta > 0, \gamma < 0$), as in the situation sketched in figure 1a. For $105 \lesssim Re < Re^{SS} \equiv 143.9$, $C_{y,\alpha}$ is also positive, indicating that θ and γ are both negative. Beyond Re^{SS}, both force projections first become negative, so that θ and γ are both positive, as in figure 1b. Then, beyond $Re \gtrsim 142$, $C_{L,\alpha}$ becomes positive again, leading back to configuration encountered for $Re \lesssim 105$. The torque coefficient $C_{M,\alpha}$ is negative for $Re < Re^{SS}$. Then it becomes positive up to a critical Reynolds number Re^{SO} where it vanishes before becoming negative again. Similar trends are observed for other aspect ratios. Table 1 provides the values of the force coefficients C_{x0}^{SO} and $C_{y,\alpha}^{SO}$ corresponding to $Re = Re^{SO}$ for various values of χ. The existence of a state with nonzero incidence and zero torque for $Re = Re^{SO}$ will later prove crucial in the situation where the body is free to move, since a steady motion then implies a zero torque.

2.4. *Orders α^2 and α^3 problems*

At order α^2, the problem and the far-field condition take the form

$$\mathcal{C}(\mathbf{u_0}, \mathbf{u}_{\alpha^2}) + \frac{1}{2}\mathcal{C}(\mathbf{u}_\alpha, \mathbf{u}_\alpha) + \nabla p_{\alpha^2} - Re^{-1}\nabla^2 \mathbf{u}_{\alpha^2} = \mathbf{0}\,,\ \nabla\cdot\mathbf{u}_{\alpha^2} = 0\,,\ \mathbf{u}_{\alpha^2} \to -\mathbf{x}/2\,. \quad (2.14)$$

Because of the structure of the solution at order α, the forcing term $\mathcal{C}(\mathbf{u}_\alpha, \mathbf{u}_\alpha)$ involves contributions with azimuthal wavenumbers $m = 0, \pm 2$. Thus the solution at order α^2 is

χ	Re^{SS}	Re^{SO}	Ar^{SO}	C_{x0}^{SO}	$C_{y,\alpha}^{SO}$	$C_{M,\alpha}^{\prime SO}$	C_{M,α^3}^{SO}
3	159.93	165.38	51.08	1.018	−2.051	−0.0919	541.975
10	130.34	143.94	46.15	1.097	−0.992	−0.0267	13.727
∞	116.75	141.67	46.54	1.102	0.590	−0.01285	−0.847
Sphere	Re^{SS}	Re^{SO}	Ar^{SO}	C_{x0}^{SO}	$C_{L,\omega}^{SO}$	$C_{M,\omega}^{\prime SO}$	C_{M,ω^3}^{SO}
	212.58	206.075	55.00	0.760	3.864	0.0173	−1193.0

TABLE 1. Critical Reynolds numbers Re^{SS} and Re^{SO}, values of the Archimedes number and the load coefficients for $Re = Re^{SO}$ for various body shapes; $C_{M,\alpha}^{\prime SO}$ (resp. $C_{M,\omega}^{\prime SO}$) is the derivative of $C_{M,\alpha}$ (resp. $C_{M,\omega}$) with respect to Re evaluated at $Re = Re^{SO}$.

sought in the form

$$\mathbf{q}_{\alpha^2} = \hat{\mathbf{q}}_2^0 + \hat{\mathbf{q}}_2^2 e^{2i\varphi} + \overline{\hat{\mathbf{q}}_2^2} e^{-2i\varphi} \quad ,$$

where $\hat{\mathbf{q}}_2^0$ and $\hat{\mathbf{q}}_2^2$ are the respective solutions of the linear problems

$$\mathcal{A}_0 \hat{\mathbf{q}}_2^0 + \left[\mathcal{C}_{1,-1}(\hat{\mathbf{u}}_1^1, \overline{\hat{\mathbf{u}}_1^1}), 0\right]^T = 0 \quad , \quad \hat{\mathbf{q}}_2^0 \to [0, 0, -1/2, 0]^T \text{ for } |\mathbf{R}| \to \infty \quad . \tag{2.15}$$

$$\mathcal{A}_2 \hat{\mathbf{q}}_2^2 + \frac{1}{2}\left[\mathcal{C}_{1,1}(\hat{\mathbf{u}}_1^1, \hat{\mathbf{u}}_1^1), 0\right]^T = 0 \quad , \quad \hat{\mathbf{q}}_2^2 \to [0, 0, 0, 0]^T \text{ for } |\mathbf{R}| \to \infty \quad . \tag{2.16}$$

Only the first of these terms contributes to the loads and results in the coefficient F_{x,α^2} through (2.5); the operators $\mathcal{A}_0$ and $\mathcal{A}_2$ are regular whatever Re. The solution at order α^3 follows a similar route; the corresponding problem and far-field condition are

$$\mathcal{C}(\mathbf{u_0}, \mathbf{u}_{\alpha^3}) + \mathcal{C}(\mathbf{u}_\alpha, \mathbf{u}_\alpha^2) + \nabla p_{\alpha^3} - Re^{-1}\nabla^2 \mathbf{u}_{\alpha^3} = \mathbf{0} \ , \ \nabla \cdot \mathbf{u}_{\alpha^3} = 0 \ , \ \mathbf{u}_{\alpha^3} \to \mathbf{x}/6 \ . \tag{2.17}$$

The solution is sought in the form

$$\mathbf{q}_{\alpha^3} = \hat{\mathbf{q}}_3^1 e^{i\varphi} + \hat{\mathbf{q}}_3^3 e^{3i\varphi} + \overline{\hat{\mathbf{q}}_3^1} e^{-i\varphi} + \overline{\hat{\mathbf{q}}_3^3} e^{-3i\varphi} \quad ,$$

where $\hat{\mathbf{q}}_3^1$ is the solution of

$$\begin{aligned} \mathcal{A}_1 \hat{\mathbf{q}}_3^1 \ + \ \left[(\mathcal{C}_{2,-1}(\hat{\mathbf{u}}_2^2, \hat{\mathbf{u}}_1^{-1}) + \mathcal{C}_{0,1}(\hat{\mathbf{u}}_2^0, \hat{\mathbf{u}}_1^1)), 0\right]^T = 0 \quad , \\ \hat{\mathbf{q}}_3^1 \to [1/12, i/12, 0, 0]^T \text{ for } |\mathbf{R}| \to \infty \quad , \end{aligned} \tag{2.18}$$

which provides the coefficient F_{x,α^3} through (2.5). The term $\hat{\mathbf{q}}_3^3$ does not contribute to the loads and hence does not need to be computed. All the above problems are non-singular provided $Re \neq Re^{SS}$, so that they are easily solved with a linear system solver.

The load coefficients at order 2 and 3 are displayed in figure 2*b* for a disk with $\chi = 10$. They are clearly highly singular for $Re \to Re^{SS}$; this is why they are plotted in logarithmic coordinates. More precisely, C_{x,α^2} exhibits a singularity of order 2 (since it results from the solution of a regular problem with a quadratic forcing term involving the solution at order 1), while C_{M,α^3} and C_{y,α^3} exhibit a singularity of order 4 (since they result from the solution of a singular problem with a forcing term with a singularity of order 3). Note that C_{x,α^2} and C_{M,α^3} are all positive in the range of Re considered, while C_{y,α^3} is negative. Similar results are obtained with other aspect ratios, except that C_{M,α^3} is found to be negative for an infinitely thin disk ($\chi = \infty$).

3. Application to freely-moving disks of various thicknesses

We now turn to the situation where the body is moving freely under the effect of buoyancy. In this case, the velocity U_0 is not imposed externally and the Reynolds number is no longer a control parameter. Therefore it is convenient to introduce the so-called Archimedes number $Ar = \nu^{-1}\{(3|m'|g)/(4\pi\rho)\}^{1/2}$, where $m'g$ is the net gravity force (including buoyancy). Conventions for this problem are sketched in figure 1*b*. Note that the angles γ and θ defined in this figure now become the slope of the path and the body inclination with respect to the vertical, respectively. An equilibrium solution for a buoyancy-driven motion requires the torque acting on the body to be zero and the hydrodynamic force to balance the buoyancy force. The latter condition provides the relation between Ar and Re, namely

$$Ar = (3/32)^{1/2}(C_x^2 + C_y^2)^{1/4} Re \quad . \tag{3.1}$$

Obviously, the axisymmetric base flow with $\alpha = \theta = \gamma = 0$ is a solution of this problem. However the weakly nonlinear expansion performed in the previous section predicts a second, nontrivial type of solution. Looking back to the last of (2.9) indicates that a solution with a zero torque and a nonzero incidence is possible provided M_α and M_{α^3} have opposite signs. For $\chi = 10$, according to figure 1 this condition is satisfied in two ranges. The first one is for $Re < Re^{SS}$ but the weakly nonlinear expansion is questionable in the vicinity of Re^{SS}, as will be seen with the sphere, so we disregard this possibility. The second range is for $Re > Re^{SO}$, leading to the branching equation defining the steady oblique (SO) solution

$$\alpha = (-M_\alpha/M_{\alpha^3})^{1/2} \tag{3.2}$$

Imposing that the corresponding hydrodynamic force be aligned with the vertical completes the determination of the solution and provides the corresponding slope and inclination angles, namely

$$\theta = -\tan^{-1}(F_y/F_x) \approx \frac{(D_0 - L_\alpha)}{D_0}\sqrt{\frac{-M_\alpha}{M_{\alpha^3}}}\ , \ \gamma = -\tan^{-1}(L/D) \approx -\frac{L_\alpha}{D_0}\sqrt{\frac{-M_\alpha}{M_{\alpha^3}}}\ . \tag{3.3}$$

Close to $Re = Re^{SO}$ and provided $C_{M,\alpha^3} > 0$, which is the case for $\chi = 10$, the leading-order approximation to (3.2) reads

$$\alpha \approx \left(-C'^{SO}_{M,\alpha}/C^{SO}_{M,\alpha^3}\right)^{1/2} \sqrt{Re - Re^{SO}} \quad , \tag{3.4}$$

where $C'^{SO}_{M,\alpha} = d(C_{M,\alpha})/d(Re)$ at $Re = Re^{SO}$ (see table 1). This is obviously a classical supercritical bifurcation equation.

Figure 3 displays α, θ and γ as predicted by (3.2) and (3.3) for disks with three different aspect ratios. For $\chi = 10$ (figure 3*a*), $Re^{SO} = 143.94$ and the critical Archimedes number is found to be $Ar^{SO} = 46.15$ (see table 1), in very good agreement with the threshold of the oblique regime, $Ar = 46.5$, determined by Auguste (2010) through direct numerical simulation for a body-to-fluid density ratio of 0.99. In this case, the slope γ is negative, meaning that the body drifts in a direction opposite to that along which it inclines with respect to the vertical. Figure 3*b* displays the same result in the case of a thicker disk with $\chi = 3$. In that case γ is positive, so that the disk drifts in the direction towards which it inclines. Such opposite behaviours of thin and thick disks were observed by Fernandes *et al.* (2007), although at higher Archimedes numbers associated with periodic fluttering. In the case of a infinitely thin disk ($\chi = \infty$), figure 3*c* shows that the bifurcation is subcritical. This stems from the fact that C_{M,α^3} is negative for $Re = Re^{SO}$, as indicated

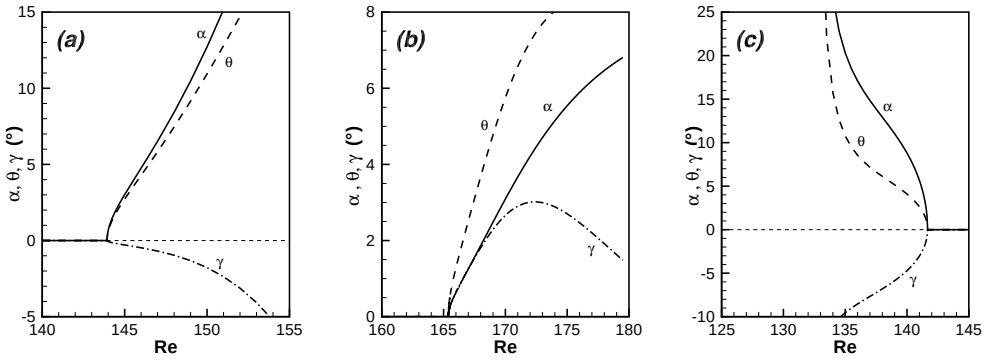

FIGURE 3. Variations with Re of the characteristic angles α, γ and θ of the weakly nonlinear solution with zero torque for $\chi = 10$ (a), $\chi = 3$ (b), and $\chi = \infty$ (c).

in table 1. Hence, close to the threshold, the leading-order solution (3.4) has to be replaced by $\alpha \approx (C'^{SO}_{M,\alpha}/C^{SO}_{M,\alpha^3})^{1/2}(Re^{SO} - Re)^{1/2}$.

Not surprisingly, Eq. (3.1) predicts that a given body (i.e. a given Ar) has a lower velocity (i.e. a smaller Re) along the SO path than along a vertical path. For instance, the Reynolds number of a body with $\chi = 10$ and $Ar = 50$ is found to be $Re \approx 150.7$ along the SO path instead of $Re \approx 159.5$ along a vertical path.

4. A freely-moving, slowly rotating sphere

We now turn to the case of a sphere for which SO paths have also been reported (Jenny *et al.* 2004; Veldhuis & Biesheuvel 2007; Horowitz & Williamson 2010). In this case the rotation rate ω (made dimensionless by normalizing the actual rotation rate with U_0/d) takes the role of the angle of incidence and we seek the solution in the form

$$\mathbf{q} = \mathbf{q}_0 + \omega\mathbf{q}_\omega + \omega^2\mathbf{q}_{\omega^2} + \omega^3\mathbf{q}_{\omega^3} + ... \tag{4.1}$$

The boundary conditions to be satisfied in the aerodynamic system of axes are

$$\mathbf{u} = \omega\mathbf{z} \times \mathbf{R} \quad \text{for} \quad |\mathbf{R}| = 1/2 \quad , \quad \mathbf{u} \to \mathbf{x}_a \quad \text{for} \quad |\mathbf{R}| \to \infty \quad . \tag{4.2}$$

The successive terms in (4.1) are computed as in section 2. The only difference lies in the boundary conditions. That is, the second (resp. first) of (4.2) applies to the base flow $\mathbf{q}_0$ (resp. to the linear correction $\omega\mathbf{q}_\omega$), while homogeneous conditions are applied to $\mathbf{q}_{\omega^2}$ and $\mathbf{q}_{\omega^3}$, both on the sphere surface and in the far field. The symmetry arguments invoked in section 2 still hold and so does (2.9), provided α is replaced by ω and F_x and F_y are replaced by D and L, respectively.

Figure 4*a* displays the load coefficients predicted by the leading-order and first-order terms in (4.1). The torque coefficient $C_{M,\omega}$ is much smaller than the other two coefficients and is thus magnified by a factor of 10 in the figure. For Reynolds numbers below Re^{SS}, the lift coefficient is negative, i.e. the lift force points towards the direction of $\omega\mathbf{e_z} \times \mathbf{U_0}$, in accordance with the classical Kutta-Joukowski argument. However, it changes sign beyond the critical Reynolds number Re^{SS} where the problem is singular and remains positive up to $Re \approx 265$ beyond which it recovers a negative sign. As for disks, the torque coefficient is found to cross zero at a single Reynolds number $Re = Re^{SO} = 206.07$. However this critical Reynolds number is smaller than the fixed-body threshold $Re^{SS} = 212.58$ for the sphere while the reverse was observed for disks. The higher-order

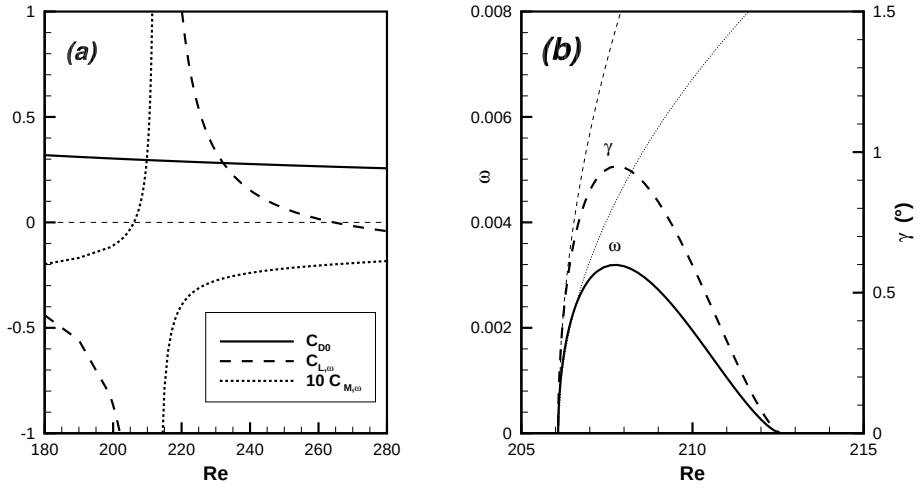

(*a*) (*b*)

FIGURE 4. Characteristics of the SO solution for a freely-moving, weakly rotating sphere. (*a*) base-flow drag coefficient and order-one lift and torque coefficients; (*b*) rotation rate ω (solid line) and slope angle γ (dashed line); in *b*, the two thin lines correspond to the expansion similar to (3.4) close to $Re = Re^{SO}$.

coefficients are not displayed in the figure; as for disks they are highly singular in the vicinity of Re^{SS} and C_{M,ω^3} is found to be negative for $Re \lesssim 245$.

As with disks, the weakly nonlinear expansion may be used to build a nontrivial steady solution of the freely-moving body problem by requiring the torque in the counterpart of (2.9) to vanish. This condition may be satisfied in the range $Re^{SO} < Re < Re^{SS}$, yielding the specific value of the rotation rate $\omega = (-M_\omega/M_{\omega^3})^{1/2}$. It may also be satisfied for $Re > 245$. However the corresponding rotation rate is found to be of order unity, so that the validity of the perturbative approach is questionable and its results are not trustworthy. The slope and inclination associated with the oblique path in the range $Re^{SO} < Re < Re^{SS}$ can be deduced from the equivalent of (3.3). The corresponding results are plotted in figure 4*b* which reveals that the rotation rate and the slope angle γ are very small. The bifurcation that takes place at $Re = Re^{SO}$ is supercritical; close to the threshold one thus has at leading order $\omega \approx (-C'^{SO}_{M,\omega}/C^{SO}_{M,\omega^3})^{1/2}(Re - Re^{SO})^{1/2}$. The numerical values of $C'^{SO}_{M,\omega}$ and C_{M,ω^3} are given in table 1 and the corresponding leading-order predictions are plotted with thin lines in figure 4*b*. In the vicinity of $Re = Re^{SS}$, the predicted rotation rate returns to zero, with a scaling of the form $\omega \propto |Re - Re^{SS}|^{3/2}$. However, as all coefficients in the expansion diverge for $Re \to Re^{SS}$, the present weakly nonlinear expansion is no longer relevant and a different approach is required to study this subregion, a point we plan to explore in the future.

The critical Archimedes number at the onset of the *SO* mode is given in table 1. Instead of *Ar*, Jenny *et al.* (2004) made use of a Galileo number defined as $2\sqrt{2}Ar$. With this definition, the critical Galileo number corresponding to the SO bifurcation is found to be 155.57, in excellent agreement with the values 155.0 and 156.1 reported by Jenny *et al.* for body-to-fluid density ratios of 0.0 and 0.5, respectively.

5. Conclusion

Using weakly nonlinear expansions of the Navier-Stokes equations, we predict the existence of steady oblique paths for two sorts of axisymmetric freely-moving bodies, namely disks of variable thickness and spheres, and describe these paths in the vicinity of the critical Reynolds number Re^{SO} corresponding to their onset. It turns out that the characteristics of these non-vertical paths do not depend on the body-to-fluid density ratio, a result that seems puzzling at first glance. However, it must be kept in mind that the whole derivation is carried out assuming the flow to be steady, so that body inertia never enters the analysis. Another remarkable result is that the value $Re = Re^{SO}$ differs from Re^{SS}, the critical Reynolds number corresponding to the onset of the steady-state wake mode for the body held fixed. However, while the SS wake mode and the SO path have apparently much in common, they actually correspond to two different situations: the SS mode has zero incidence and a nonzero torque (and lift), while the SO solution has zero torque and a nonzero incidence. The SO solution having been obtained through an asymptotic approach, its validity when $|Re - Re^{SO}|$ increases is unknown and will have to be checked against results of full numerical simulations. An investigation based on such simulations would be of special interest in the case of the sphere, for which the weakly nonlinear method fails to predict the existence of the SO path beyond $Re^{SS} \approx 212.6$, although such paths have been reported in this range of Re. Finally, although the SO path is an equilibrium solution for a given body geometry irrespective of the body-to-fluid density ratio, the stability of this solution certainly depends on this ratio; this problem will be considered in a future work.

We thank the conceivers of the FreeFem++ software for having built such a powerful tool. We also acknowledge Denis Sipp and Philippe Méliga for having designed the smart notation system used in section 2, and Flavio Giannetti for stimulating discussions.

REFERENCES

Auguste, F. 2010 Instabilités de sillage générées derrière un corps solide cylindrique fixe ou mobile dans un fluide visqueux. PhD thesis, Université de Toulouse, France.

Chrust, M., Bouchet, G. & Dusek, J. 2010 Parametric study of the transition scenario in the wake of oblate spheroids and flat cylinders. *J. Fluid Mech.* **665**, 199–208.

Ern, P., Risso, F., Fabre, D. & Magnaudet, J. 2012 Wake-induced oscillatory paths of bodies freely rising or falling in fluids. *Annu. Rev. Fluid Mech.* **44**, 97–121.

Fabre, D., Assemat, P. & Magnaudet, J. 2011 A quasi-static approach to the stability of the path of heavy bodies falling within a viscous fluid. *J. Fluids Struct.* **27**, 758–767.

Fabre, D., Auguste, F. & Magnaudet, J. 2008 Bifurcation and symmetry breaking in the wake of axisymmetric bodies. *Phys. Fluids* **20**, 051702.

Fernandes, P. C., Risso, F., Ern, P. & Magnaudet, J. 2007 Oscillatory motion and wake instability of freely-rising axisymmetric bodies. *J. Fluid Mech.* **573**, 479–502.

Horowitz, M. & Williamson, C. H. K. 2010 The effect of Reynolds number on the dynamics and wakes of freely rising and falling spheres. *J. Fluid Mech.* **651**, 251–294.

Jenny, M., Dusek, J. & Bouchet, G. 2004 Instabilities and transition of a sphere falling or ascending freely in a Newtonian fluid. *J. Fluid Mech.* **508**, 201–239.

Meliga, P., Chomaz, J.-M. & Sipp, D. 2009 Global mode interaction and pattern selection in the wake of a disk: a weakly nonlinear expansion. *J. Fluid Mech.* **633**, 159–189.

Natarajan, R. & Acrivos, A. 1993 The instability of the steady flow past spheres and disks. *J. Fluid Mech.* **254**, 323–344.

Veldhuis, C. H. J. & Biesheuvel, A. 2007 An experimental study of the regimes of motion of spheres falling or ascending freely in a Newtonian fluid. *Int. J. Multiphase Flow* **33**, 1074–1087.